Advances in the characterization of pressures and velocities in the overtopping of arch and gravity dams

L.G. Castillo[1], J.M. Carrillo[1] and F. Marco[2]

[1] *Dept. of Civil Engineering. "Hidr@m" Group of R & D & i. Universidad Politécnica de Cartagena (UPCT)*
Paseo Alfonso XIII, 52, 30203 Cartagena. Spain

Abstract

When dams overflow, they produce free jets that discharge into plunge pool basins. The pressure and velocity distributions of the flow in the plunge pool must be estimated to evaluate the potential scour that might destabilize the dam. In Protections 2016 event (Fort Collins, Colorado, USA), the first two authors presented results of free falling jets in plunge pool, comparing numerical results against experimental data. Instantaneous pressures, velocities and air entrainment were obtained with piezoresistive transducers, Acoustic Doppler Velocimeter and optical fiber, respectively. To identify the level of reliability of models, numerical simulations were carried out by using the "homogeneous" model of ANSYS CFX, together with different turbulence closures. Castillo et al. (2015) established different equations to calculate the jet energy dissipation in the air and in the water cushion, as a function of the Y/B_j and H/L_b ratios (where Y and H denote the depth of the water cushion at the plunge pool and the total head, respectively, and L_b is the break-up length). This paper includes further measurements that complete the range of flow tested. New adjustments and analysis are presented in the mean, fluctuating and extreme dynamic pressure coefficients. Furthermore, velocity and turbulent kinetic energy profiles have been obtained. The energy dissipation in the air and in the plunge pool has been also analyzed.

1 Introduction

Current capacity of many spillways is inadequate, raising the possibility that dams might be overtopped during extreme events.

The energy dissipation mechanisms can be grouped into the following: (a) aeration and disintegration of the jet in its fall, (b) air entrainment and diffusion of the jet into the basin, (c) impact on the basin bottom, and (d) recirculation in the basin (see Figure 1).

Issuance conditions correspond to the flow conditions at a location where the jet leaves the spillway and starts falling freely. In the arch dam case, issuance conditions are located at z=-h, where z is the vertical coordinate with origin in the crest weir, and h is the weir head. Similarly, in the gravity dam case conditions are also considered at z=- h. The impingement conditions correspond to the jet section before the impact with the water surface of the basin. In this location, the mean velocity, V_j, and the impingement jet thickness, B_j, must be defined. Figures 1a and 1b show the overtopping on an arch and gravity dam, respectively. When the jet falls through a long-enough distance, the jet becomes fully developed (L_b).

Figure 1. Schematic of falling rectangular jets and receiving basin. (a) Overtopping on an arch dam. (b) Overtopping on a gravity dam.

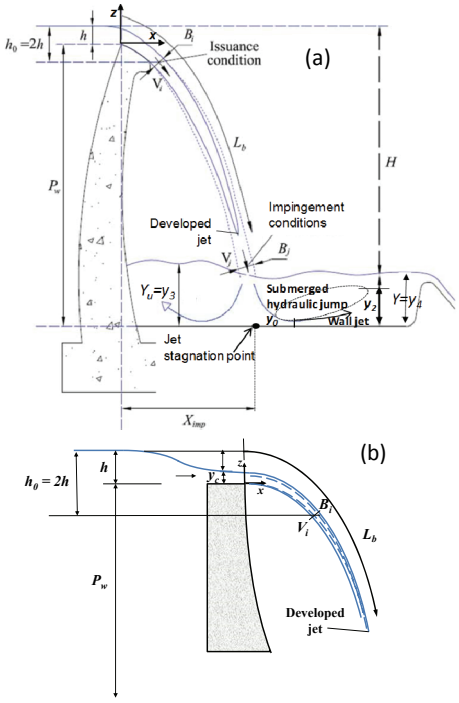

Appendix 1 summarizes the formulations of the main characteristics of rectangular jets.

2 Experimental facility

The experimental facility was constructed at the Hydraulics Laboratory of the Universidad Politécnica de Cartagena, and was described in detail in Carrillo and Castillo (2014). The facility consists of a mobile mechanism which permits to vary the weir height between 1.7 and 3.5 m, and flows from 10 to 150 l/s. It has an inlet channel with a length of 4.0 m and width of 0.95 m. The discharge is produced through a sharp-crested weir with a width of 0.85 m and height of 0.37 m. The plunge pool, in which different water cushions may be simulated, is a 1.3-m high, 1.1-m wide and 3.0-m long methacrylate box. Turbulent kinetic energy values at the inlet channel were obtained with an Acoustic Doppler Velocimeter (ADV); mean velocities and air concentrations in different sections of the falling jet were acquired with optical fiber instrumentation; and instantaneous pressure values were measured with piezoresistive transducers located on the basin bottom. In addition, ADV and optical fiber were used in the basin to obtain velocity and air concentration profiles, respectively, downstream of the impingement point. Figure 2 shows a picture of the experimental device in which sizable values of air concentration are apparent.

Figure 2. Device of turbulent jet.

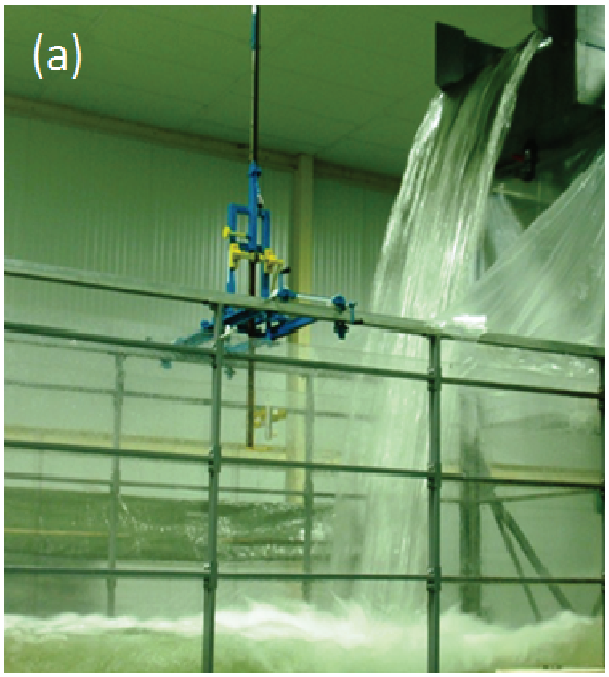

3 Pressures characterization around of the stagnation point

3.1 Mean and fluctuating dynamic pressures coefficients

Castillo et al. (2015) established different equations to calculate the jet energy dissipation in the air and in the water cushion, as a function of the Y/B_j and H/L_b ratios (where Y and H denote the depth of the water cushion at the plunge pool and the total head, respectively).

In non-effective water cushions (Y/B_j<5 for the rectangular jet case), the energy dissipates due to the air entrainment during the fall of the jet and the water depth in the plunge pool generated upstream of the jet. Figure 3 shows the mean dynamic pressure coefficient on the basin bottom and the air energy dissipation as a function of the falling height to break-up length ratio (H/L_b).

Figure 3. Mean dynamic pressure coefficient C_p and air energy dissipation ED as a function of H/L_b ratio for non-effective water cushions.

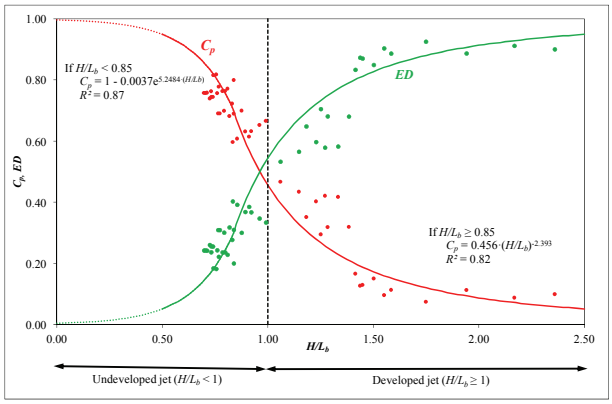

Energy dissipation in the basin by diffusion effects appears if there is an effective water cushion (Y/B_j>5 for the rectangular jet case). Figures 4 and 5 show the mean and fluctuating dynamic pressure coefficient as a function of the Y/B_j and H/L_b ratios, respectively.

These dynamic pressure coefficients may be used as estimators of the stream power reduction coefficients. Hence, the effect of the jet disintegration in the air and their diffusion in the stilling basin may be considered.

Figures 6, 7 and 8 show the mean dynamic pressure distribution around of the stagnation point. The developed jets (H/Lb>1) have a greater pressure distribution region than undeveloped jets (H/Lb≤1). Aki (1969) formula (b_{distib}=0.13Y) is more extended than the envelope of the mean dynamic pressures proposed by the other authors.

Figure 4. Mean dynamic pressure coefficient Cp as a function of H/Lb and Y/Bj ratios.

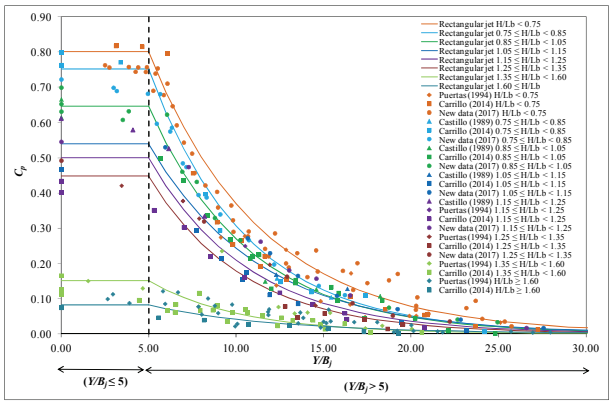

These dynamic pressure coefficients may be used as estimators of the stream power reduction coefficients. Hence, the effect of the jet disintegration in the air and their diffusion in the stilling basin may be considered.

Figure 5. Fluctuating dynamic pressure coefficient C_p' as a function of H/L_b and Y/B_j ratios.

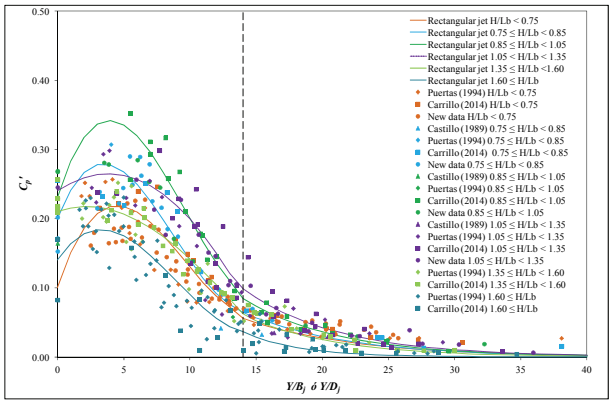

The Cola (1966), Aki (b_{distib}=0.23Y proposed by Xu Duo-Ming & Yu Chang-Zhao, 1983), Hartung & Häusler (1973) when y_k=7.2B_j , and Beltaos (1976) formulae were obtained for a non-aerated jets. Their results are in agreement with the lower envelope of the data obtained in the laboratory (with a smaller aeration). The Hartung & Häusler distribution (when y_k=5B_j) shows results between those proposed by the other authors.

Through using the same general expression (see Appendix 1), different upper envelopes have been obtained. For $H/L_b \leq 1$, a parameter ϕ=10 has been obtained. For H/L_b>1, the jets are very aerated and the influence region greater, obtaining a parameter ϕ=7.

Ervine et al. (1997) considered the variation of the mean dynamic pressure coefficient as a function of the water cushion (see Appendix 1).

Figure 6. Mean dynamic pressure distribution as a function of the pressure influence region, $b_{distrib}$.

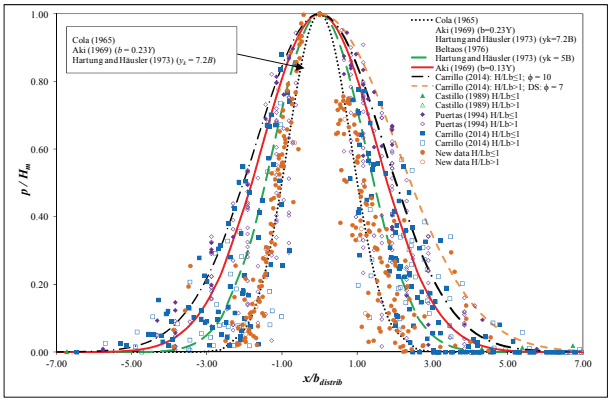

The parameter K_2 varies from 30 for shallow pool depths ($Y/D_j \leq 4$) to 50 for greater pool depths. The distribution is valid for $H/L_b \leq 0.5$ and it is in agreement with the rectangular jet results obtained when the jet is less aerated. For the rectangular jets with $H/L_b \leq 1$, a parameter K_2=7 has been obtained. For H/L_b>1, the jets are highly aerated and the influence region is greater, obtaining a value of the K_2=4 (see Figure 7).

Figure 7. Mean dynamic pressure distribution as a function of the water cushion, Y.

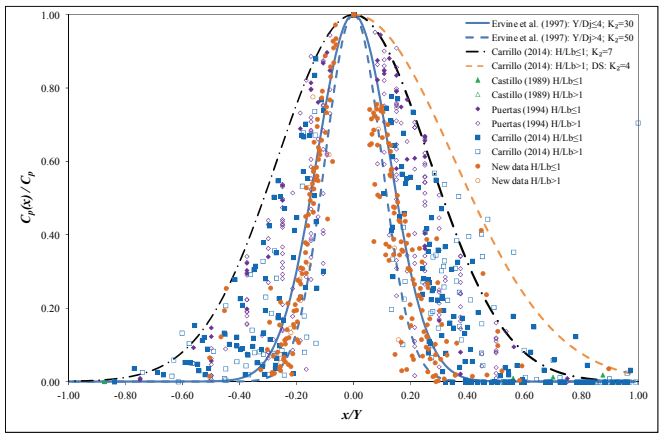

Bollaert (2002) considers the longitudinal distribution of the mean dynamic pressure coefficient as a function of maximum longitudinal distance extension of the area influenced by the turbulent shear layer of the impacting jet, x_{max}=0.5D_j+0.25Y. For the circular jet case, the parameter K_3 varies from 3 for shallow pool depths to 6 for greater pool depths (Figure 8).

The Bollaert distributions are valid for H/L_b<0.5 and are in agreement with the rectangular jet results obtained when the jet is less aerated. Thus, for rectangular jets with $H/L_b \leq 1$, a parameter of K_3=0.60 has been obtained. For H/L_b>1, the jets are highly aerated and the influence region is greater, with the downstream parameter K_3=0.40 (see Figure 8).

Figure 8. Mean dynamic pressure distribution as a function of the influence area by the incident jet turbulent shear layer, x_{max}.

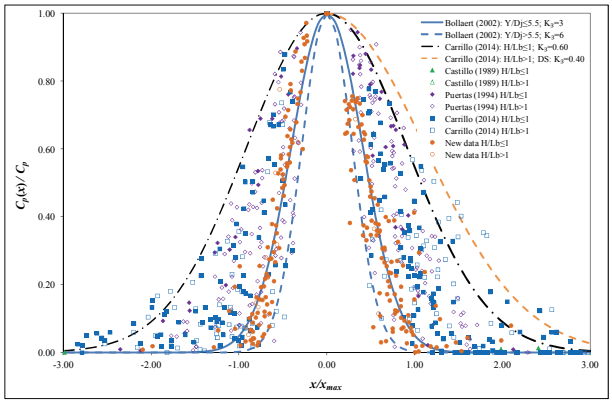

3.2 Extreme pressures

Magnitudes are highly dependent on extreme value distributions, in turn depending upon the turbulence characteristics in the pool and the length of time of the observations. As a practical matter, Lopardo (1988) recommended the use of a 1% exceedance value as the cut-off limit for design purposes. The maximum C_p^+ and minimum C_p^- fluctuating pressure coefficients have been obtained. However, the values have not permitted the study to establish any type of grouping. Figures 9 and 10 show the maximum and minimum coefficient values, including the envelopes of the pairs 1–99% and 5–95% cut-off limits, respectively.

Figure 9. Variation of the maximum pressure coefficient with the plunge pool depth.

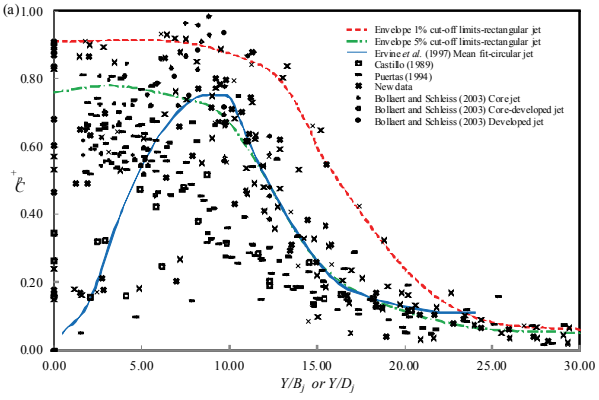

The C_p^+ and C_p^- values are in agreement with previously published data corresponding to the circular jet case (Bollaert & Schleiss, 2003; Ervine et al., 1997). Comparison with Figure 5 shows that the maximum positive pressure fluctuations are nearly two to three times greater than the RMS values, while the maximum negative pressure fluctuations are around twice such values.

Figure 10. Variation of the minimum pressure coefficient with the plunge pool depth.

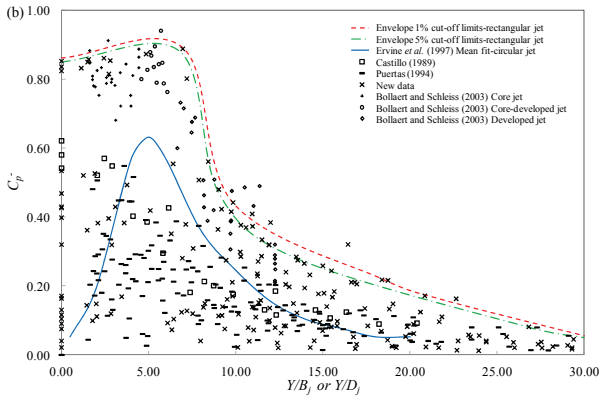

Figures 11 and 12 indicate the adjustments of the maximum dynamic instantaneous pressures (P_{max}/H) and the maximum amplitudes of the pressure fluctuations ($2A_m/H$) as a function of the water cushion to the critical depth (Y/y_c) ratio, respectively.

Figure 11. Maximum dynamic instantaneous pressures on the stagnation point.

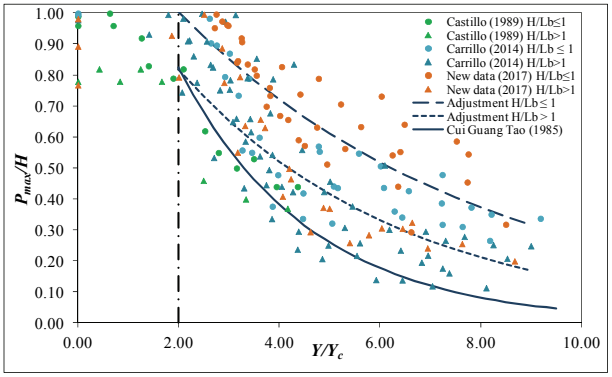

With the new data and for $Y/y_c \geq 2$ ratios, two independent adjustments have been obtained for undeveloped flows ($H/L_b \leq 1$) and fully developed flows ($H/L_b > 1$). Cui Guang Tao (1985) adjustment constitutes a lower limit of the developed and highly aerated jets.

Figure 12. Maximum pressure amplitudes on the stagnation point.

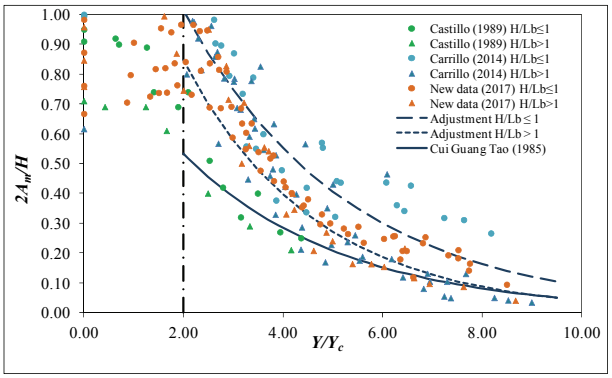

3.3 Flow characterization in the basin

Within the plunge pool downstream of the impingement point, the flow resembles a flow in a wall jet and a submerged hydraulic jump (Figure 13). However, the situation is complicated to measure due to the air entrainment.

Figure 13. Velocity distribution for submerged jumps.

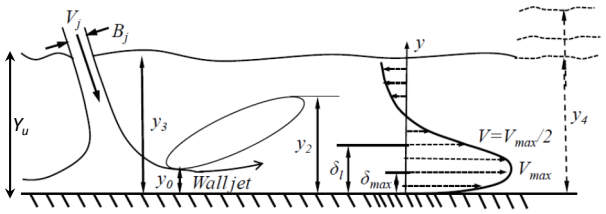

Considering the water cushion depth under the nappe, Y_u, and P_w as the vertical distance from the weir to the bottom of the dissipation basin, Figure 14 shows the laboratory results of the head loss coefficient β adjustment for the ratio Y/P_w. The β value is approximately 0.6 for plane jet case and 0.55 for a three-dimensional jet case.

Figure 14. Head loss coefficient β as a function of Y/P_w.

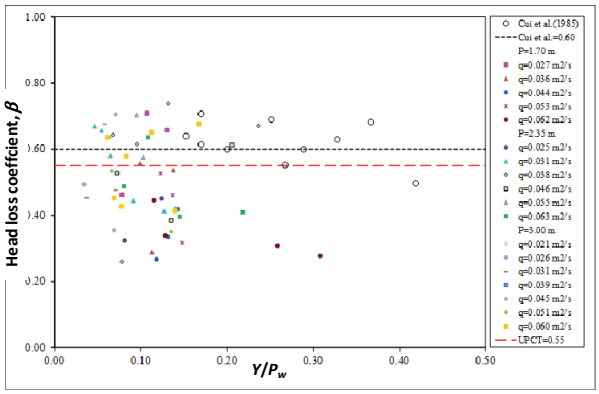

Figure 15 shows the velocity profiles in different cross sections located downstream of the stagnation point. Measurements were performed with Doppler and optical fiber equipment and were compared with the results of the CFD simulations (Castillo et al., 2017). The velocities have been non-dimensioned using the maximum horizontal velocities in each cross section, V_{max}. In general, the results of the numerical simulations show the same behavior as the values obtained in the laboratory.

Figure 16 shows the turbulent kinetic energy (TKE) obtained in different sections of the plunge pool with the ADV equipment. The turbulent kinetic energy tends to dissipate quickly as the flow moves away from the impact zone. The results obtained with the CFD simulation follow the evolution of the energy dissipation (Castillo et al. 2017).

Figure 15. Horizontal velocity in different sections of the plunge pool (q=0.082 m^2/s, H=2.19, Y=0.32 m).

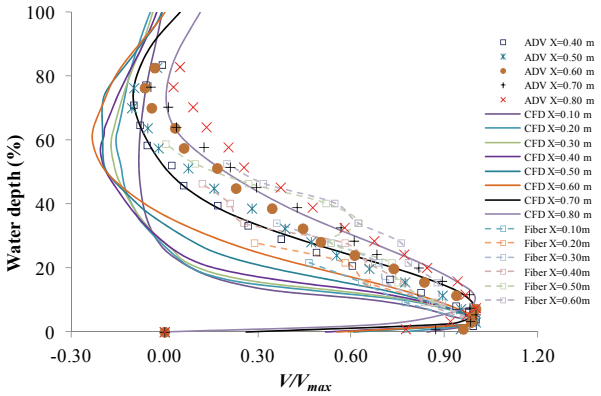

Figure 16. Turbulent kinetic energy in different sections of the plunge pool (q=0.082 m^2/s, H=2.19, Y=0.32 m).

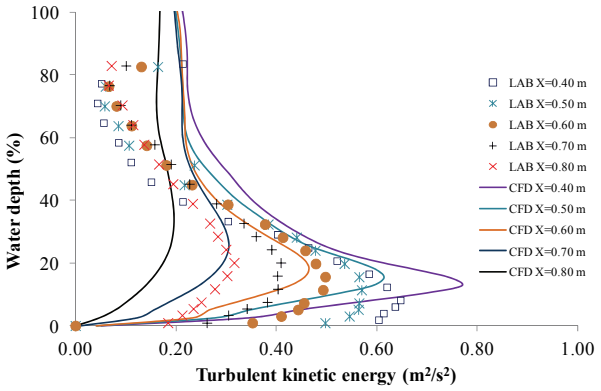

Figure 17 shows the non-dimensional velocity profiles obtained from the numerical simulations as well as the ADV measurements for several tests.

Results are quite similar to the profiles obtained with the formulae proposed by several authors. Due to the strong recirculation with air entrainment, in the upper side of the submerged hydraulic jumps there is a bigger scatter for ratios V_x/V_{max}<0.40.

Figure 17. Velocity distribution downstream of the stagnation point (x≥0.40 m).

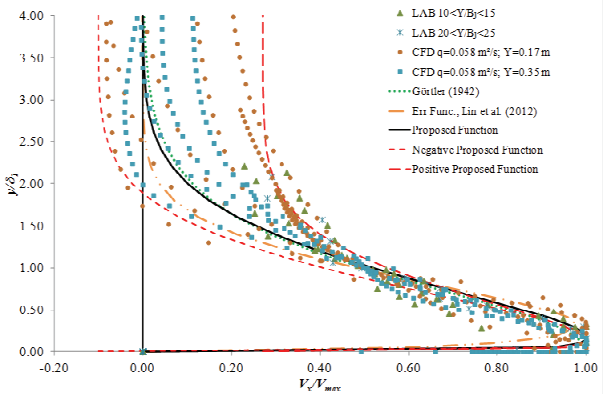

Figure 18 shows the comparison between the relative energy dissipation and the Froude number at the impingement conditions, $F_j=V_j/(gB_j)^{1/2}$, obtained from experiments.

Figure 18. Relative energy dissipation in the plunge pool as a function of the impingement Froude number.

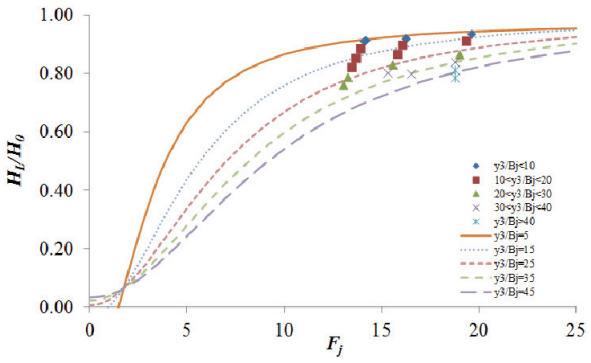

In the laboratory device, the impingement Froude number is between 13 and 20 for the impingement jet thickness of 0.015 m plotted in Figure 19. In general, tests carried out show values of energy dissipation larger than 75% of the impingement jet energy. This ratio increases when the ratio y_3/B_j decreases.

Figure 19. Relative energy dissipation in the plunge pool as a function of the ratio y_3/B_j for the case B_j=0.015 m.

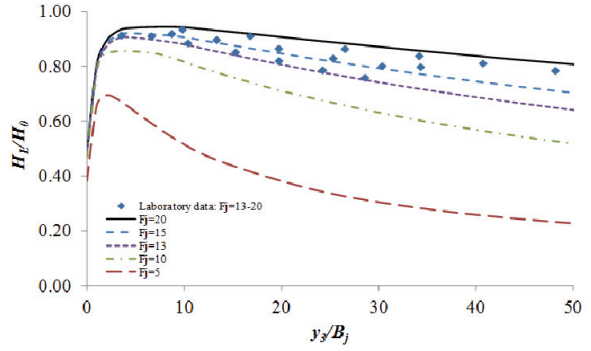

4 Conclusions

The energy dissipation in a plunge pool is very high. For the tests carried out, the dissipation of the impingement jet energy was between 75 and 95 %. This ratio increases when the ratio y_3/B_j decreases.

The new pressure measurements confirm previous studies in rectangular and circular falling jets.

In general, the CFD simulations provided results fairly close to the values measured in the laboratory, and to the formulas proposed by several authors. It was possible to propose a single mean velocity distribution law for ratios $V_x/V_{max}\geq 0.40$. For smaller values, there are necessarily diverse distribution laws.

In the case of extreme pressures it has been possible to obtain two independent adjustments for undeveloped ($H/L_b\leq 1$) and fully developed ($H/L_b>1$) flows.

To extrapolate to prototypes, the designer should take the scale effects into account. To err on the side of safety, the authors consider that these scale effects would not be relevant until a Froude scale is of 1:10.

In order to develop this work, we plan to examine air entrainment in the stilling basin.

References

Aki, S. (1969). Study on fluctuating characteristics of water dynamic force acting on base of free overfall. CRIEPI Research Report No. 69009 [in Japanese].

Beltaos, S. (1976). "Oblique impingement of circular turbulent jets". Journal of Hydraulic Research, 14(1), 17–36.

Bollaert, E. F. R., & Schleiss, A. J. (2003). "Scour of rock due to the impact of plunging high velocity jets Part II: Experimental results of dynamic pressures at pool bottoms and in one- and two-dimensional closed end rock joints". Journal of Hydraulic Research, 41, 465–480.

Carrillo, J. M. (2014). Metodología numérica y experimental para el diseño de los cuencos de disipación en el sobrevertido de presas de fábrica (PhD Thesis). Departamento de Ingeniería Civil, Universidad Politécnica de Cartagena, Spain.

Castillo, L. (1989). Metodología experimental y numérica para la caracterización del campo de presiones en los disipadores de energía hidráulica. Aplicación al vertido libre en presas bóveda (PhD Thesis). Departamento de Ingeniería Hidráulica, Marítima y Ambiental, Universidad Politécnica de Cataluña, Spain.

Castillo, L., Puertas, J., & Dolz, J. (1999). Discussion of 'Pressure fluctuations on plunge pool floors' by D. A. Ervine, H. T. Falvey & W. A. Withers. Journal of Hydraulic Research, 37, 272–288.

Castillo, L. (2006). Aerated jets and pressure fluctuation in plunge pools. Proceedings of the Seventh International Conference on Hydroscience and Engineering (ICHE-2006), Philadelphia, 1–23, M. Piasecki and College of Engineering, Drexel University, USA.

Castillo, L., Puertas, J., & Dolz, J. (2007). Discussion of 'Scour of rock due to the impact of plunging high velocity jets. Part I: A state-of-the-art review' by E. F. R. Bollaert & A. J. Schleiss. Journal of Hydraulic Research, 45, 853–858.

Castillo, L., Carrillo, J. M., & Sordo-Ward, A. (2014). Simulation of overflow nappe impingement jets. Journal of Hydroinformatics, 16(4), 922–940.

Castillo, L.G., Carrillo, J.M., and Blázquez, A. (2015). "Plunge pool mean dynamic pressures: a temporal analysis

in nappe flow case". *Journal of Hydraulic Research,* 53(1), 101–118.

Castillo, L.G., Carrillo, J.M., and Bombardelli, F.A. (2017). "Distribution of mean flow and turbulence statistics in plunge pools". *Journal of Hydroinformatics,* 19(2), 173-190. DOI: 10.2166/hydro.2016.044.

Cola, R. (1966). Diffusione di un getto piano verticale in un bacino d'aqua d'altezza limitata. L'Energia Elettrica, 11, 649–667 [in Italian].

Cui Guang Tao, Lin Ji Yong, & Liang Xing Rong (1985). "Study on the force and effect of the Arch dam overflow water tongue on the river bed". *Journal of Hydraulic Engineering*, Beijing 8, 53–68 [in Chinese].

Ervine, D. A., Falvey, H. T. & Withers, W. A. (1997). "Pre sure fluctuations on plunge pool floors". *J. Hydraul. Res.* 35(2), 257–279.

Hartung, F., & Häusler, E. (1973). Scours, stilling basins and downstream protection under free overfall jets at dams. Proceedings of the 11th Congress on Large Dams, Madrid, Spain, 39–56.

Görtler, H. 1942. Berechnung von Aufgaben der freien Turbulenz auf Grund eines neuen Näherungsansatzes. *Journal of Applied Mathematics and Mechanics / ZAMM*, 22(5), 244–254, (in German).

Lopardo, R. (1988). Stilling basin pressure fluctuations. Proceedings of the International Conference on Model Prototype Correlation in Hydraulic Structures, Colorado Springs, Colorado, 56–73.

Manso, P. A., Bollaert, E. F. R., & Schleiss, A. J. (2008). Evaluation of high-velocity plunging jet-issuing characteristics as a basis for plunge pool analysis. Journal of Hydraulic Research, 46, 147–157.

Puertas, J. (1994). Criterios hidráulicos para el diseño de cuencos de disipación de energía en presas bóveda con vertido libre por coronación (PhD Thesis). Departamento de Ingeniería Hidráulica, Marítima y Ambiental, Universidad Politécnica de Cataluña, Spain.

Wu, S., and Rajaratnam, N. (1996). "Transition from hydraulic jump to open channel flow." *Journal of Hydraulic Engineering,* 122(9), 526–528.

Appendix 1. Summary of the formulations of the main characteristics in plunge pools.

FORMULAE	OBSERVATIONS
Castillo et al. (2015, 2016) and some modifications proposed in this paper. **Issuance conditions:** $\frac{L_b}{B_i F_i^2} = \frac{K}{(\varphi F_i^2)^{0.82}}$ $L_b = \frac{C_d^{0.82} h^{0.73}}{2g^{0.68}\varphi^{0.82}} K$ **Impingement conditions:** $B_j = B_g + 2\xi$ $B_j = \frac{q}{\sqrt{2gH}} + 4\varphi\sqrt{h}\left[\sqrt{2H} - 2\sqrt{h}\right]$ **Mean dynamic pressure (C_p):** If $Y / B_j \le 5$ and $H / L_b < 0.85$ $C_p = 1 - 0.0037 e^{5.2484(H/L_b)}$ If $H/L_b \ge 0.85$: $C_p = 0.456(H/L_b)^{-2.393}$ If $Y / B_j > 5$: $C_p = \frac{H_m - Y}{V_j^2/2g} = a e^{-b(Y/B_j)}$	L_b jet break-up length B_i issuance conditions jet thickness F_i issuance conditions Froude Number $K \approx$ 0.85, fit coefficient; $\varphi = K_\varphi T_u$, turbulence parameter K_φ turbulence coefficient. 1.24 (arch dam); 1.20 (gravity dam) T_u turbulent intensity issuance conditions. 0.012 (arch dam); 0.013 (gravity dam) C_d discharge coefficient. 2.1 (arch dam); 1.70 (gravity dam) h weir head ξ jet lateral spreading B_j impingement jet thickness q specific flow H height between upstream water level and downstream water level $g \approx 9.8$ m/s^2, gravity acceleration H_m head mean registered at plunge pool bottom (stagnation point) Y depth at plunge pool V_j mean velocity in impingement conditions

H / L_b	a	b	R^2	C_p ($Y/B_j < 5.5$)
< 0.75	1.740	-0.155	0.893	0.802
0.75-0.85	1.850	-0.180	0.921	0.752
0.85-1.05	1.550	-0.175	0.868	0.646
1.05-1.15	1.200	-0.160	0.822	0.539
1.15-1.25	1.200	-0.175	0.836	0.500
1.25-1.35	1.130	-0.185	0.731	0.448
1.35-1.60	0.390	-0.190	0.749	0.151
≥1.60	0.160	-0.135	0.722	0.081

<table>
<tr><th>FORMULAE</th><th>OBSERVATIONS</th></tr>
<tr><td>

Fluctuating dynamic pressure (C'_p):

$$C'_p = \frac{H'}{V_j^2/2g}$$

$Y / B_j < 14$:

$$C'_p = a\left(\frac{Y}{B_j}\right)^3 - b\left(\frac{Y}{B_j}\right)^2 + c\left(\frac{Y}{B_j}\right) + d$$

$Y / B_j \geq 14$:

$$C'_p = a\left(\frac{Y}{B_j}\right)^b$$

</td><td>

H' root mean square of instantaneous pressures

V_j jet impingement velocity

H / L_b	a	b	c	d
< 0.75	0.0003000	-0.0086	0.0590	0.100
0.75-0.85	0.0003400	-0.0090	0.0500	0.200
0.85-1.05	0.0003450	-0.0100	0.0625	0.230
1.05-1.35	0.0000005	-0.0017	0.0130	0.240
1.35-1.60	0.0000300	-0.0017	0.0070	0.210
> 1.60	0.0002000	-0.0054	0.0290	0.140

H / L_b	a	b	R^2
< 0.75	0.30	0.12	0.72
0.75-0.85	0.40	0.13	0.76
0.85-1.05	0.60	0.14	0.66
1.05-1.35	0.70	0.14	0.70
1.35-1.60	0.50	0.15	0.81
> 1.60	1.05	0.24	0.75

</td></tr>
<tr><td>

Extreme instantaneous pressure

Cui Guang Tao (1985), Castillo (1989)

$Y/y_c < 2$: $\frac{P_{max}}{H} = 0.90$; $\frac{2A_m}{H} = 0.85$

$Y/y_c \geq 2$: $\frac{P_{max}}{H} = 0.68^{[(Y/y_c)-1.5)]}$; $\frac{2A_m}{H} = 0.73^{(Y/y_c)}$

New data (2017)

$H/L_b \leq 1$: $\frac{P_{max}}{H} = 1.395e^{-0.165(Y/y_c)}$

$\frac{2A_m}{H} = 1.865e^{-0.305(Y/y_c)}$

$H/L_b > 1$: $\frac{P_{max}}{H} = 1.285e^{-0.226(Y/y_c)}$

$\frac{2A_m}{H} = 1.810e^{-0.380(Y/y_c)}$

Pool depth under nappe

$$Y_u / Y = \sqrt{1 - 2F_D[(V_j/V_D)\beta\cos\theta - 1]}$$

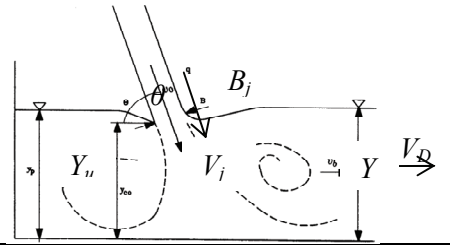

</td><td>

P_{max} maximum instantaneous pressure

P_{min} minimum instantaneous pressure

$2A_m = P_{max} - P_{min}$. *maximum pressure amplitude*

Y_u pool depth under nappe

Y water cushion

$F_D = V^2_D / (gY)$ square Froude number

V_j impingement velocity

V_D downstream velocity

β head loss coefficient:

plane jet ≈ 006

tridimensional jet ≈ 0.55

θ, impingement jet angle

</td></tr>
<tr><td>

Mean pressure distribution around of the stagnation point

Cola (1966), Aki (1969), Hartung and Hausler (1973), Beltaos (1976), Castillo (1989), Castillo et al. (2015):

$$\frac{p}{H_m} = e^{-\phi\left(\frac{x}{b_{distrib}}\right)}$$

Circular jet. Ervine et al. (1997):

$$\frac{C_p(x)}{C_p} = e^{-K_2\left(\frac{x}{Y}\right)^2}$$

Circular jet. Bollaert (2002):

</td><td>

p mean dynamic pressure distribution

H_m mean dynamic pressure on the stagnation point

ϕ adjustment parameter

$b_{distrib}$ width of the pressure influence region. Distance between the upstream and downstream points where $p=H_m/2$

Cola: ϕ =0.685; $b_{distrib}$=0.13Y

Aki: ϕ =0.664; $b_{distrib}$=0.23Y

Hartung and Hausler: ϕ =0.688; $b_{distrib}$=0.13Y

Beltaos: ϕ =0.693; $b_{distrib}$=0.13Y

Circular jet:

$Y / D_j \leq 4$; $K_2 = 30$

$Y / D_j > 4$; $K_2 = 50$

Rectangular jet

$Y / B_j \leq 5$; $K_2 = 30$

$Y / B_j > 5$; $K_2 = 50$

Circular jet: $x_{max} = 0.5Dj+025Y$

$Y / D_j \leq 5.5$; $K_3 = 3$

</td></tr>
</table>

FORMULAE	OBSERVATIONS
$\frac{C_p(x)}{C_p} = e^{-K_3\left(\frac{x}{x_{max}}\right)^2}$	$Y / D_j > 5.5$; $K_3 = 6$ Rectangular jet: $x_{max} = 0.5Bj+025Y$ $Y / B_j \leq 5$; $K_3 = 2.5$ $Y / B_j > 5$; $K_3 = 5.5$
Submerged hydraulic jump Castillo et al. (2015, 2016, 2017) Wall jet: $\frac{V_x}{V_{max}} = 1.48\left(\frac{y}{\delta_l}\right)^{1/7}\left(1 - erf\left(0.66\frac{y}{\delta_l}\right)\right)$ Negative recirculation flow: $\frac{V_x}{V_{max}} = 1.65\left(\frac{y}{\delta_l}\right)^{1/7}\left(1 - erf\left(0.72\frac{y}{\delta_l}\right)\right) - 0.10$ All the flow downstream $\frac{V_x}{V_{max}} = 1.10\left(\frac{y}{\delta_l}\right)^{1/7}\left(1 - erf\left(0.80\frac{y}{\delta_l}\right)\right) + 0.27$	V_x horizontal mean velocity at a x distance downstream from the stagnation point V_{max} horizontal maximum mean velocity δ_l distance from the bottom when $V=V_{max}/2$ y distance from the bottom
Energy dissipation in the basin $\frac{H_L}{H_0} = \frac{2\left(\frac{y_3}{y_0} - \frac{y_4}{y_0}\right) + \left(1 - \frac{1}{(y_4/y_0)^2}\right)F_{r0}^2}{2(y_3/y_0) + F_{r0}^2}$	H_L total energy dissipation H_0 energy upstream of the hydraulic jump y_o contracted depth upstream of the hydraulic jump y_3 water depth upstream of the hydraulic jump y_4 tailwater downstream of the hydraulic jump F^2_{L0} Froude number upstream of the hydraulic jump